

Response to the reviewer

The motivation for the 20-year length of the analyzed period.

Page 5, line 9-14 Authors write “The twenty-year time slices were chosen to align the hydrodynamic model output to wave model simulations described in Hemer and Trenham [2016] with the aim to combine hydrodynamic extremes with wave-induced extremes (e.g. wave setup or runup) in future work.”

To me this looks a weak justification: having a longer period would not have prevented this planned future work

We changed the text significantly, both in the section 2.3 indicated by the reviewer, and in the concluding section to make justification clearer, with appropriate caveats.

And further “The 20-year time slices are deemed adequate for assessing how large scale circulation changes will affect the drivers of ESLs around much of the Australian coast where seasonally varying weather systems are a major cause of extreme sea levels.” I think this is also weak as extreme weather frequency is affected by multidecadal variability. Could references be added to support that “20-year time slices are deemed adequate“?

See previous, response – also we have expanded reasoning about where (spatially) uncertainties may be high/low.

Neglecting of the tide-surge component, is acceptable because their computation would have been expensive, and benefits on climate change detection arguable, however:

Page 5 at line 20-21 authors write " [tide-surge interaction] may impact substantially on an individual surge event, [but] it does not change the surge statistics over a period of years to decades" . If it impacts significantly individual events, why it has no effect on the statistics? Even though it will not change the mean surge level, it would make the distribution broader or narrower, therefore eventually, increasing ordecreasing extreme values

Yes, we changed the sentence to make this clearer. The statistics don't change dramatically for most of Australia's coastline. Some changes are observed for selected stations such as Broome, Darwin and Burnie where maximum surges tend to be systematically underestimated/ overestimated for ranges of maximum SLA (Figure 6).

Further, (figure 4) extreme surges are underestimated in the model simulation and this might explain why tide-surge interaction is weak

This is a possibility.

At Line 1-2 at page 8 “some evidence points towards this peak being generated by a coastally trapped wave (CTW).” ...It is not clear what is the evidence.

The evidence is discussed later in the paragraph. We added a notion in the sentence to make it more clear.

At line 17 page 3

The conclusions Lionello et al are not reported fully (just read the last sentence in the abstract of that paper). The sentence “, but mass addition will likely determine an increase of the water level maxima” should be added

OK – we extended the sentence as suggested by the reviewer.

1 **Atmospheric Circulation Changes and their Impact on Extreme Sea Levels**
2 **around Australia**

3
4
5
6
7
8
9
10
11
12
13
14
15
16
17
18
19
20
21
22
23
24
25
26
27
28
29
30
31
32
33

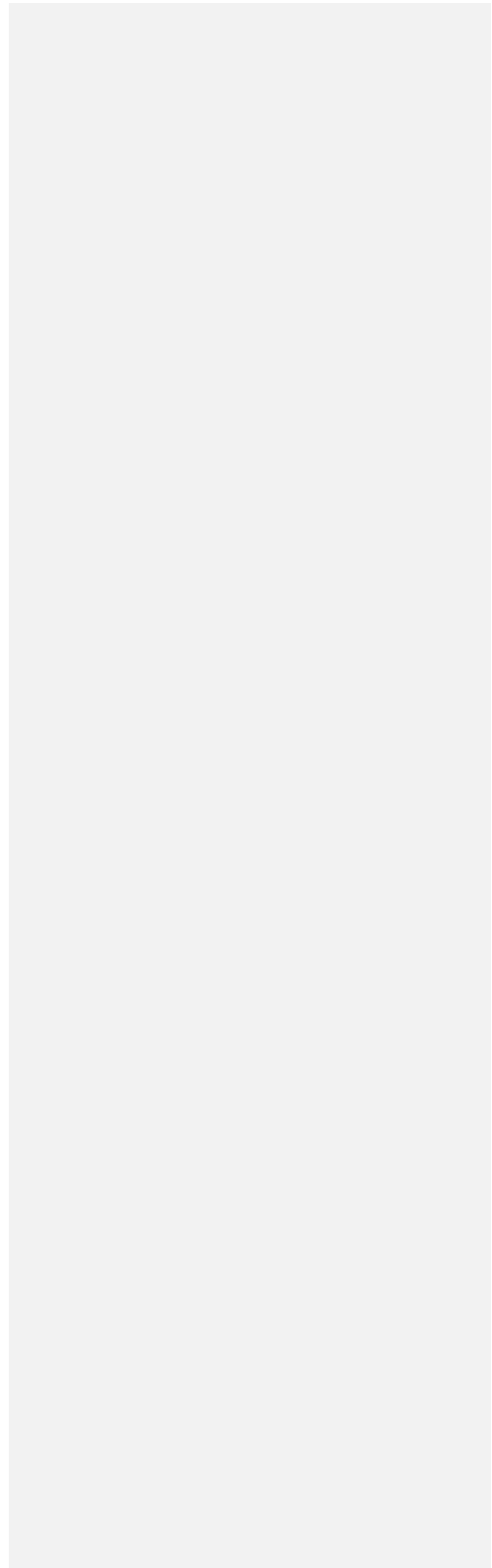
Frank Colberg¹, Kathleen L. McInnes², Julian O’Grady² and Ron Hoeke²

¹Bureau of Meteorology,
f.colberg@bom.gov.au

²Climate Science Centre,
CSIRO Marine and Atmospheric Research,
Aspendale, 3195, Australia
kathleen.mcinnes@csiro.au
julian.ogrady@csiro.au
ron.hoeke@csiro.au

Revised November 2018

Journal: Natural Hazards and Earth System Sciences (NHESS)



34 **Abstract**

35

36

37

38 Projections of sea level rise (SLR) will lead to increasing coastal impacts during extreme sea level events
39 globally, however, there is significant uncertainty around short-term coastal sea level variability and the
40 attendant frequency and severity of extreme sea level events. In this study, we investigate drivers of coastal
41 sea level variability (including extremes) around Australia by means of historical conditions as well as future
42 changes under a high greenhouse gas emissions scenario (RCP 8.5). To do this, a multi-decade hindcast
43 simulation is validated against tide gauge data. The role of tide-surge interaction is assessed and found to have
44 negligible effects on storm surge characteristic heights over most of the coastline. For future projections,
45 twenty-year long simulations are carried out over the time periods 1981-1999 and 2081-2099 using
46 atmospheric forcing from four CMIP5 climate models. Changes in extreme sea levels are apparent but there
47 are large inter-model differences. On the southern mainland coast all models simulated a southward
48 movement of the subtropical ridge which led to a small reduction in sea level extremes in the hydrodynamic
49 simulations. Sea level changes over the Gulf of Carpentaria in the north are largest and positive during
50 Austral summer in 2 out of the 4 models. In these models, changes to the northwest monsoon appear to be the
51 cause of the sea level response. These simulations highlight a sensitivity of this semi-enclosed gulf to changes
52 in large scale dynamics in this region, and indicate that further assessment of the potential changes to the
53 northwest monsoon in a larger multimodel ensemble be investigated, together with its effect on extreme sea
54 levels.

55

56

Deleted: .

1. Introduction

Extreme sea levels (ESLs) are a significant hazard for many low-lying coastal communities [Hanson *et al.*, 2011; Nicholls *et al.*, 2011] and with rising global mean sea level, extreme events are expected to rise [Menéndez and Woodworth, 2010]. ESLs are largely driven by storm surge superimposed on the astronomical tides (storm tides). The severity of these ESLs can be further enhanced by larger-scale atmospheric and oceanic circulation patterns that operate on seasonal to interannual time scales.

ESL hazards are typically represented as probability-based exceedance levels with associated uncertainties. These uncertainties may be significantly larger than uncertainties in projected SLR itself [Wahl *et al.*, 2017]. Many studies have attempted to quantify ESL uncertainties using historical tide gauge information combined with global SLR projections [e.g. Hunter, *et al.*, 2013], or by spatially extrapolating tide gauge observations using a hydrodynamic model [e.g. Haigh *et al.*, 2014a]. In the present study, we assess the performance of a hydrodynamic model for the Australian region and examine atmospheric drivers of ESL and how they may change under future climate conditions.

A number of studies have used a similar approach, i.e. investigating ESL changes using hydrodynamic models forced by global climate models (GCMs) or regional climate models (RCMs). Lowe *et al.* [2009] developed projections of storm surge change for the UK using climate forcing from an 11-member perturbed physics ensemble of the Hadley Centre GCM downscaled to 25 km resolution with the RCM HadRM3 [Murphy *et al.*, 2007] under a mid-range SRES [Nakićenović and Swart, 2000] emission scenario. Results indicated that the changes in the 2 to 50-year storm surge height associated with projected changes in weather and storms would increase by no more than 0.09 m by 2100 anywhere around the UK coast. [Sterl *et al.*, 2009] concatenated the output from a 17-member ensemble of a mid-range SRES emissions scenario from the ECHAM5/MPI-OM climate model [Jungclaus *et al.*, 2006] to estimate 10,000-year return values of surge heights along the Dutch coastline. No statistically significant change in this value was projected for the 21st century because projected wind speed changes were associated with non-surge generating south westerlies rather than surge-conducive northerlies. Vousdoukas *et al.* (2016) used a hydrodynamic model to downscale storm surge changes in an 8-member ensemble of climate models under RCP 4.5 and 8.5 and found increases in storm surges over the model domain north of 50°N whereas there was minimal to slightly negative change south of 50°N except under RCP 8.5 towards the end of the century. In southern Europe, Marcos *et al.* [2011] assessed changes in storm surges in the Mediterranean Sea and Atlantic Iberian coasts using climate model forcing from the ARPEGE-v3 global, spectral stretched-grid climate model under a high, medium and low SRES emissions scenario [Jordà *et al.*, 2012]. Findings revealed a general decrease in both the frequency and magnitude of storm surges with up to a 0.08 m reduction in the 50-year return levels. In southern Australia Colberg and

93 *McInnes* [2012] found both positive and negative changes in 95th percentile sea level height across the
94 southern half of the Australian continent in surge model simulations forced by the high SRES emission
95 scenario of the CSIRO Mark 3.5 GCM [*Gordon et al.*, 2010] and two simulations of the CCAM stretched grid
96 global model [*McGregor and Dix*, 2008]. The ESL changes were small, mostly negative along the southern
97 mainland coast but with wintertime increases over Tasmania. These resembled the changes in wind patterns to
98 some degree, although there were large inter-model differences.

99
100 Several studies have also examined the non-linear effect of rising sea levels on tide and surge propagation.
101 Using a global tide model, *Pickering* [2017] found that changes in mean high tide levels exceeded $\pm 10\%$ of
102 the SLR at approximately 10% of coastal cities when coastlines were held fixed, but a reduction of tidal range
103 when coastlines were allowed to recede due to resulting changes in the period of oscillation. *Arns et al.* [2015]
104 investigated the non-linear impact of SLR on maximum storm surge heights in the North Sea, focussing on the
105 German Bight. They found that maximum storm surges relative to the imposed background sea levels were
106 amplified by up to 20% when the background mean sea levels were elevated by around 0.5 m. The positive
107 increases in extreme water levels were caused by nonlinear changes in the tidal component, which were only
108 partially offset by a reduction in the storm surge component.

109
110 Coastal regions affected by tropical cyclones have been the focus of several recent studies. For example,
111 *Umnikrishnan et al.* [2011] used RCM simulations to force a storm-surge model for the Bay of Bengal and
112 found that the combined effect of mean SLR of 4 mm yr^{-1} and RCM projections for the high emissions
113 scenario (2071– 2100) gave an increase in 1-in-100 year heights in the range of 15–20% compared to the
114 1961–1990 baseline. For east Asia, *Yasuda et al.* [2014] applied a hydrodynamic model based on a 20-km
115 resolution climate model and found that storm surge heights increased in the future for much of the coastline
116 considered. For New York, *Lin et al.* [2012] investigated the change in extreme sea levels arising from
117 hurricanes over 2081-2100 relative to 1981-2000 in four GCMs run with the SRES medium emission scenario
118 by generating synthetic cyclones under the background conditions provided by the GCMs. Accounting for
119 hurricane forcing only, results differed markedly between the four climate models ranging from overall
120 increases to decreases in storm surge level. *McInnes et al.* [2014, 2016a] used a synthetic cyclone technique to
121 investigate the effect of a 10% increase in cyclone intensity and a frequency reduction of 25% (consistent with
122 tropical cyclone projections for the region) on storm tides over Fiji and Samoa and found a reduction in storm
123 tides with return periods of less than 50 years and an increase for return periods longer than 200 years.

124
125 In new studies, the contribution of waves to extreme sea levels as well as storm surge and sea level rise has
126 also been examined. For Europe, *Vousdoukas et al.* (2017) using a 6-member ensemble of climate models to
127 assess changes in extreme sea levels, found that by 2100, under RCP 8.5, Changes in storm surges and waves
128 enhance the effects of SLR along the majority of northern European coasts by up to 40% whereas for southern

Deleted: R

130 Europe, decreases in storm surges and waves tend to offset the increases in extreme sea levels due to mean sea
131 level rise. For the Mediterranean, *Lionello et al.*, (2017) used a 7-member ensemble of regional climate model
132 simulations under the SRES A1B scenario to examine sea level changes by 2050 and found that the positive
133 contribution to sea level extremes of the ~~steric (thermal expansion) component of SLR~~ would be largely offset
134 by the declining trend in storms and hence storm surges and waves over this time period. ~~However, mass~~
135 ~~addition (melting of land ice) component of SLR will likely determine an increase of water level maxima~~. In
136 a global study, *Vousdoukas et al.*, (2018) shows that under RCP4.5 and RCP8.5, the global average 100-year
137 extreme sea level arising from mean sea level, tides, wind-waves and storm surges is very likely to increase by
138 34-76 cm and 58-172 cm, respectively between 2000 and 2100.

139
140 Numerical modelling studies of the non-linear interactions between sea level rise and cyclone-induced
141 extreme water levels due to tides, storm surge and waves have also been undertaken. Smith et al. [2010]
142 showed that sea level rise altered the speed of propagation of tropical cyclone-induced storm surges on the
143 south-eastern Louisiana coast and amplified the extreme water levels under SLR although the amount of
144 amplification varied significantly along different parts of the coast. Hoeke et al. [2015] found that SLR
145 reduced wave setup and wind setup by 10-20% but increased wave energy reaching the shore by up to 200%
146 under cyclone conditions along the Apia, Samoa coastline.

147
148 Australia extends from the tropics to the mid-latitudes with a variety of meteorological systems responsible
149 for extreme sea levels along its coastline [*McInnes et al.*, 2016b]. The range of weather systems, and more
150 particularly their associated spatial scales means that it is challenging to obtain meteorological forcing that
151 consistently represents all weather systems responsible for sea level extremes. *McInnes et al.*, [2009, 2012,
152 2013] used joint probability methods to evaluate ESLs in southeastern Australia. *Haigh et al.*, [2014a; 2014b]
153 extended such modelling and analysis of ESLs to the entire Australian coast, using two approaches. In *Haigh*
154 *et al.*, (2014a), the water levels arising from weather and tides were investigated over the period 1949 to 2009
155 using 6-hourly meteorological forcing obtained from the NCEP reanalyses while in *Haigh et al.*, (2014b),
156 ESLs were simulated using a synthetic cyclone approach. As expected, extreme sea levels over the tropical
157 northern coastlines were underestimated in the first study compared to the second one because of the low
158 resolution of tropical cyclones in the reanalysis data set.

159
160 The present study assesses the performance of a medium resolution barotropic hydrodynamic model for the
161 Australian region to investigate extreme sea levels for the current climate and examines for the first time over
162 the entire Australian coastline the potential changes in a future climate scenario in a four-member ensemble of
163 climate model simulations. The model described by *Colberg and McInnes* [2012] is extended to cover the
164 entire Australian coastline at 5 km resolution. A current climate (baseline) simulation is undertaken with tide
165 and atmospheric forcing over the period 1981-2012 using reanalyses from the NCEP Climate Forecast System

Formatted: Font: (Default) Times New Roman, 11 pt

Deleted: positive

Deleted: trend in thermal expansion

Deleted: the

Deleted:

170 Reanalyses (CFSR) [Saha *et al.*, 2010]. The performance of the model is assessed with respect to tides,
171 weather driven sea levels, and tide-surge interaction. Finally, changes are investigated in storm surge and
172 seasonal sea levels around the coastline based on forcing from an ensemble of four CMIP5 models forced with
173 the RCP 8.5 emission scenario [Taylor *et al.*, 2012].

174
175 The paper is organised as follows. Section 2 describes the model setup, input data sets and procedure for
176 assessing model performance. Section 3 assesses the model performance and the baseline simulations are used
177 to investigate tide-surge interaction around the Australian coastline and the meteorological causes of ESLs.
178 Section 4 presents the results from simulations forced by climate models and section 5 discusses the results,
179 conclusions and further work.

180

181 2. Model Description and Method

182

183 2.1 Model Configuration

184

185 As with Colberg and McInnes [2012], the model used in this study is the Rutgers version of the Regional
186 Ocean Modeling System (ROMS) [Shep^etkin and McWilliams, 2005] configured to run in barotropic or
187 ‘depth-averaged’ mode. The model grid spans the region shown in Figure 1 at 5 km resolution. Bathymetry
188 for the model is obtained from the 1’x1’ resolution General Bathymetric Chart of the Oceans data set
189 [GEBCO, Jakobsson, *et al.*, 2008].

190

191 For simulations including tides, the tidal currents and heights were derived from the TPXO7.2 global model
192 (Egbert *et al.*, 1994; Egbert and Erofeeva, 2002) and applied to the open model boundaries. TPXO7.2 best fits
193 (in a least-squares sense) the Laplace Tidal Equations and along track-averaged data from the
194 TOPEX/Poseidon and Jason altimetry missions, obtained with OTIS (Oregon State University Tidal Inversion
195 Software). Eight primary tidal constituents (M2, S2, N2, K2, K1, O1, P1, Q1) are provided on a 1/4 of a
196 degree resolution full global grid. A combination of Flather/Chapman boundary conditions was used in
197 applying the tidal forcing [Flather, 1976; Chapman, 1985]. The Flather condition was applied to the normal
198 component of the barotropic velocity and radiates deviations from the values at exterior grid points out of the
199 model domain at the speed of the external gravity waves. The corresponding Chapman condition for surface
200 elevation assumes all outgoing signals leave at the shallow-water wave speed. Meteorological forcing is
201 discussed in the next section.

202

203 **2.2 Baseline experiment**

204

205 In the first part of the study, we assess the ability of the Australia-wide ROMS model to simulate historical
206 tides and meteorologically-driven water levels. The model experiments performed are also used to investigate
207 non-linear tide-surge interactions as well as the meteorological causes of extreme sea levels around the
208 Australian coastline. Three baseline experiments are run over the period 1981-2012. The first experiment, B-
209 TM, includes tidal and meteorological forcing, the second, B-T, tide-forcing only and the third, B-M,
210 meteorological forcing only. Meteorological forcing for these experiments is obtained from the Climate
211 Forecast System Reanalyses (CFSR) dataset [*Saha et al., 2010, Saha et al., 2014*], which provides
212 meteorological variables across the globe at hourly temporal resolution and approximately 38 km spatial
213 resolution from 1979 to 2012.

214

215 **2.3 Climate change experiments**

216

217 Finally, a set of simulations with meteorological forcing from four GCMs from the 5th Phase of the Coupled
218 Model Intercomparison Project (CMIP5; [*Taylor et al, 2012*]) is undertaken to assess how climate change will
219 affect sea levels around the Australian coast. [Sub-daily data, which is necessary for the climate simulations](#)
220 [undertaken in this study, was archived only for selected 20-year time slices from the late 20th to the late 21st](#)
221 [Century in the CMIP5 experiment.](#) Four models were chosen by subjectively evaluating performance metrics
222 reported by *Hemer & Trenham* [2016] as well as computational considerations and data availability (see [Table](#)
223 [1 for details](#)). The 20-year time slices are deemed adequate for assessing how large-scale circulation changes will
224 affect the drivers of ESLs around much of the Australian coast where seasonally varying weather systems are a
225 major cause of extreme sea levels. [This may not be the case in areas where El Niño Southern Oscillation \(ENSO\) is](#)
226 [associated with significant interannual sea level variability, however this is confined largely to Australia's northern](#)
227 [coastline westward from the Gulf of Carpentaria and is minimal on the east and southern coasts \[e.g. see Figure 2a](#)
228 [in *McInnes et al, 2016*\].](#)

229

230 Tides were not included in the simulations forced by climate models. This was primarily because of the large
231 computational overhead required to undertake two simulations for each time slice (current and future)
232 consisting of one simulation with tides only and one with tides and atmospheric forcing in order to calculate
233 non-tidal residuals. As will be discussed in section 3.3, the decision to omit tidal forcing from the climate runs
234 is somewhat justified because non-linear tide-surge interaction is evident around parts of Australia and
235 therefore may impact substantially on an individual surge event it does not change the surge statistics over a
236 period of years to decades [significantly for most locations around Australia](#) [*Williams et al., 2016*], which is

Deleted: The various experiments are described in Table 1. The f

Deleted: ,

Deleted: The twenty-year time slices were chosen to align the hydrodynamic model output to wave model simulations described in *Hemer and Trenham* [2016] with the aim to combine hydrodynamic extremes with wave-induced extremes (e.g. wave setup or runup) in future work.

Deleted:

Deleted: A major source of

Deleted: on interannual time scales is caused by El Niño Southern Oscillation (see *McInnes et al, 2016*; see for example Figure 2a) but

Deleted: . The various experiments are described in Table 1.

Formatted: Font: Italic

Deleted: tide

254 the main focus of the experiments. In the following we refer to the climate change simulations as CC (see also
255 Table 1).

256

257 3. Baseline results and model performance

258

259 Here we assess the baseline experiments (forced by CFSR and/or tides) in terms of how well the model-
260 generated sea levels compared with observations. In the first sub-section, we address the contribution of
261 seasonal and interannual variability in sea level in the modelled and observed data. The following sub-sections
262 examine the performance of the model in representing astronomical tides, the high frequency variability in sea
263 levels including extremes, and the meteorological drivers of ESLs around the coast. Finally, we examine tide-
264 surge interaction.

265

266 The model is assessed against hourly tide measurements from fourteen high quality tide gauges from the
267 Australian Base Line Sea Level Monitoring Network with data available from 1993 to 2012 (Figure 1). We
268 decompose both the tide gauge measurements and the simulated sea levels at corresponding model grid points
269 in the B-TM simulation into components consisting of the (a) seasonal and interannual variability, (b) the tidal
270 signal and (c) the residual signal (the remaining signal after the removal of the seasonal and tidal components
271 from the total sea level) using the approach of *Haigh et al.* [2014a]. In order to facilitate a fair comparison
272 between modelled and observed time series we apply the same methodology to both. Firstly, sea levels are
273 linearly de-trended at each station. The seasonal and interannual component is then derived by applying a 30-
274 day running mean to the detrended time series. The running mean is removed in the next step and a harmonic
275 tidal analysis is carried out using T-Tide [*Pawlowicz et al.*, 2002]. This yields the tidal signal. Removing the
276 tidal signal from the time series gives the residuals which include the storm surge signal. .

277

278 These component time series, as well as the total sea level, are compared by means of root mean square errors
279 (RMSE), The mean difference in standard deviation between observations and simulation (STDE) and linear
280 correlations between the modelled and observed time series over the period from 1993 to 2012 (the shorter
281 assessment period is determined by the availability of tide gauge data at the selected sites). In addition, a 1-
282 day running mean filter was applied to the de-tided modelled and observed sea levels for the locations of
283 Darwin and Broome because these locations display high frequency intra-daily to daily variability in sea
284 surface height after applying the filtering techniques described above. This variability may be a consequence
285 of the large tidal signal in the area propagating over a fairly shallow and wide shelf. The nature of the high
286 frequency variability is such that at times it would mask surge events related to atmospheric weather patterns.

287 **3.1 Seasonal and interannual variations in sea level**

288 Table 2 compares the differences between the seasonal signal in the observations and the model via RMSE,
289 STDE and correlation coefficients. For most of the coastline, the RMSE values are 0.07 m or less with lowest
290 values along the southeast coast. Higher values of RMSE occur on the northern and western coastline from
291 Milner Bay (0.15 m) to Hillarys (0.10 m). Similarly, STDE indicate that the model underestimates the
292 seasonal component by a larger amount in these locations. The reason for the poorer model performance in
293 these locations may be attributed to seasonal and interannual variations since these regions feature a relatively
294 large steric component, which is not simulated by barotropic models [Haigh *et al.*, 2014a].

295

296 In Milner Bay, a large seasonal cycle in sea level occurs in part due to the transition from the prevailing north-
297 westerly winds during the December to April monsoon to the dry season southeasterly trade winds from May
298 to November [Oliver and Thompson, 2011; Green *et al.*, 2010] and steric effects from seasonal variations in
299 ocean temperature and salinity. Variations in barotropic and steric sea level components are approximately in
300 phase, are at a maximum in January and are highest in the southeast of the Gulf of Carpentaria [Forbes and
301 Church, 1983].

302 The range of the seasonal signal from tide gauge measurements for Milner Bay is estimated here to be 0.67 m.
303 This is lower than the range of approximately 0.8 m reported in Tregoning *et al.* [2008] based on five years of
304 data and the difference may be a result of interannual variations in the seasonal cycle in the longer record that
305 is analysed here. The range of the seasonal signal in the barotropic model is 0.27 m, also smaller than the
306 barotropic range of 0.4 m estimated by Tregoning *et al.* [2008]. Nevertheless, the results highlight that the
307 steric component contributes to about half of the seasonal variation in sea levels in the Gulf of Carpentaria.

308 A relatively large steric component is also present in the seasonal signal from Darwin to Hillarys and this is
309 related to seasonal variations in the strength of the southward flowing Leeuwin Current, which is weakest in
310 October to March as it flows against maximum southerly winds and is strongest between April and August
311 when southerly winds are weaker [Godfrey and Ridgway, 1985]. This produces an annual cycle in sea levels at
312 Hillarys of about 0.22 m with maximum levels occurring in May-June and minimum levels in October-
313 November [Pattiaratchi and Eliot, 2008]. The range of the seasonal signal from the Hillarys tide gauge is
314 estimated here to be 0.34 m whereas in the model it is 0.09 m, the difference being of a similar order to the
315 steric effect, which is not captured by the model.

316 **3.2 Tides**

317 A comparison of the amplitudes of the eight major tidal constituents derived from the measured and modelled
318 sea levels over 1993-2012 is presented in Figure 2 for each of the tide gauge locations. For most locations
319 there is reasonably good agreement between constituents estimates from model and observations. The largest

320 differences in the M2 and S2 constituents occur along the south coast at Thevenard and Port Stanvac. At Port
321 Stanvac in particular, this may be related to poor resolution of tidal waves propagating into the Gulf of St.
322 Vincent. Milner Bay in the Gulf of Carpentaria is also showing poor agreement, with the leading O1 and K1
323 constituents largely underestimated by the model. The RMSE values in Table 2 also reflect larger differences
324 and lowest correlations at Port Stanvac and Thevenard. Locations with large tidal amplitudes such as Broome
325 and Darwin display the largest RMSE errors (30 and 40cm respectively). On average RMSE, STDE and
326 correlation across all locations is 0.17 m, -0.05 m and 0.94 respectively indicating generally good model skill
327 overall.

328 3.3 Sea Level Residuals

329 The sea level residuals, obtained after removal of the tides and seasonal signal are indicative of short-term
330 fluctuations such as storm surge. Table 2 shows error statistics for the sea level residuals over the period 1993
331 to 2009 and in Figure 3 data is plotted for selected sites for the year 1997. This particular year is selected
332 because it contained examples of storm surges at each of the tide gauge locations across the Australian region.
333 The lowest RMSE errors of around 0.06 m are generally located along the east coast and within Bass Strait.
334 The largest RMSE errors of 0.11 m are found at Milner Bay in the Gulf of Carpentaria and at Thevenard and
335 Port Stanvac along the south coast. Correlations are highest at gauges across the south coast stretching from
336 Hillarys to Spring Bay with values exceeding 0.8 at all locations except Burnie where a slightly lower
337 correlation of 0.77 was found. Correlations are lowest in macro-tidal areas with large shelves and/or complex
338 bathymetry, with the lowest values of 0.55 and 0.39 at Darwin and Broome respectively. The poorer
339 performance in these areas are further demonstrated using quantile-quantile plots shown in Figure 4. It can be
340 seen that the ESLs tend to be more systematically underestimated along this coastline than in the southern
341 mid-latitudes. For example, at Milner Bay the 99.9th percentile values are underestimated by approximately
342 0.5 m. At Port Stanvac, the underestimation of the high percentiles is likely a result of the 5 km grid spacing
343 of the model inadequately resolving the Gulf of St. Vincent in which Port Stanvac is located.

344 To provide further insights into the type and scale of the synoptic weather systems responsible for the storm
345 surge events identified by arrows in Figure 3 (note that for Burnie, the synoptic map for Portland applies),
346 Figure 5 presents the mean sea level pressure (MSLP) and 10 m wind vectors at the time of the peak sea
347 levels. At Spring Bay, the peak residual of 0.4 m on 8 July 1997 is associated with the passage of a frontal
348 trough that brings low pressure and southwesterly winds along the eastern Tasmanian coast (Figure 5a).
349 *McInnes et al. [2012]* found that daily maximum sea levels at Spring Bay were highly correlated with those in
350 Hobart ($r=0.98$) and Portland ($r=0.80$) indicating the strong influence of frontal systems on sea level extremes
351 in this part of the country. Indeed relative peaks in residuals are evident at other south mainland coast stations
352 for this event (Figures 5g-j).

Deleted: the

354 At Port Kembla a relative peak in residual sea level of 0.3 m at around 10 May 1997 is the result of an east
355 coast low that brings southeasterly winds to the coast. These systems are the cause of the majority of elevated
356 sea level events along this coastline [McInnes and Hubbert, 2001]. A tropical cyclone off the northeast coast
357 around 9 March (Figure 3c and 5c) and in the Gulf of Carpentaria on 28 December are responsible for sea
358 level residuals of up to 0.4 at Rosslyn Bay and 1.0 m at Milner Bay respectively (Figure 3d and 5d). A second
359 residual peak at Rosslyn Bay of up to 0.4 m around 13 May was not captured by the model.

360 The cause of this peak in the observations is not easily explained by the synoptic winds and SLP fields.
361 However, some evidence, [as described next](#), points towards this peak being generated by a coastally trapped
362 wave (CTW). Coastally trapped waves travel anticlockwise around Australia with speeds between 2-4m/s and
363 amplitudes in the order of 0.25m (Woodham et al., 2013). On May 10th a coastal low produced a surge in Port
364 Kembla that may have excited such a CTW. The timing and measured elevation height for the peak at Rosslyn
365 Bay matches well with theoretical values of a passing CTW. The barotropic hydrodynamic model used in this
366 study does not allow higher order (baroclinic) modes of CTW to exist and this may contribute to the failure of
367 the model to capture this extreme sea level. Also unresolved bathymetric features over the Great Barrier Reef
368 may alter the modelled sea surface height signal at this location.

369 At Darwin, a small relative peak of about 0.2 m around 22 February is associated with a burst of northwest
370 monsoon winds (Figures 3e and 5e). At this time sea levels are also elevated to 0.5 m at Milner Bay (Figure
371 3d) by the northwesterly winds that are also directed into the Gulf of Carpentaria. At Hillarys, a sea level peak
372 around 18 May is associated with a low pressure system off the southwest of the continent directing
373 northwesterly flow onto the southwest coast. The final sequence of figures (Figures 5g-i) show the passage of
374 a cold front that travels from west to east bringing southwesterly winds to the south coast of Australia and
375 producing elevated sea levels in Esperance on 04 June (Figure 3g and 5g), Thevenard on 05 June (Figure 3h
376 and 5h) and Portland and Burnie on 06 June (Figures 3i-j, 5i). Events of this type have been discussed in
377 previous studies such as *McInnes and Hubbert*, [2003] and *McInnes et al.*[2009].

378 **3.4 Tide-surge interaction**

379 Understanding tide-surge interaction is important since it can alter timing, severity and intensity of storm
380 surges [Olbert et al., 2013; Haigh et al., 2014b, Antony and Unnikrishnan, 2013]. In the context of the present
381 study, a better understanding of the potential non-linear interaction between tides and surges contributes to an
382 understanding of the uncertainty associated with the CMIP5-forced ocean model simulations.

383 Tide-surge interaction has been studied previously for parts of the Australian coast. In Bass Strait, the
384 occurrence of strong westerly winds leads to a phase shift in the timing of the surge [McInnes and Hubbert,
385 2003; Wijeratne et al., 2012]. On the northern shelf, the combination of strong tropical cyclone winds together
386 with tides alters the amplitude of the water column [Haigh et al., 2014b]. Both of these observed effects are in
387 line with the notion of [Rossiter, 1961] that the interaction of tides and surges is one of mutual alteration.

Deleted: 4

389 Simply put, depending on the size of the tide and the water depth the presence of tides alters the generation of
390 the surge signal because the wind is more effective at creating a surge over lower sea levels. They conclude
391 therefore that surges produced during low tide are generally larger [Horsburgh and Wilson, 2007] than those
392 produced during high tides. Furthermore, since the tide and surge signals propagate as shallow water waves
393 the presence of a surge increases the speed of the tidal wave so that the high tide arrives sooner than predicted.
394 Therefore, when predicted tides are removed from tide gauge observations, the residuals can contain
395 variations that are not driven by meteorological effects [e.g. McInnes and Hubbert, 2003].

396 To examine tide-surge interaction, sea level components (ζ) from the three baseline simulations are analysed
397 (see Table 1). The first is forced by meteorology (B-M, i.e. atmospheric winds and pressure only) yielding
398 surge only, ζ_M ; the second (B-T) is forced by tides only, ζ_T ; and the third (B-TM) combines tide and
399 meteorological forcing, ζ_{TM} . Subtracting the ζ_T from the ζ_{TM} yields a time series of residuals ζ_R . By definition,
400 differences between the time series of residuals and surges (i.e. ζ_R and ζ_M) are a result of tide-surge
401 interaction.

402 The potential amplitude changes arising from tide-surge interactions around Australia are first examined by
403 selecting the four largest surges and the four largest residuals (separated by a 3-day window) per year from the
404 20-year ζ_M and ζ_R time series respectively and ranking the values (Figure 6). Although ranking of events
405 removes the one-to-one relationship between the events in the surge and residual time series, it clarifies the
406 relationship between the two. Figure 6 suggests the relationship between the surges and residuals (red points
407 and axes on top and right) are close to one, indicating that across the population of extremes the height of the
408 surge is not systematically affected by the presence of tides in B-TM. Exceptions are Broome, where the
409 largest residuals (those greater than 0.6 m) are higher than the equivalent surges and Darwin and Burnie where
410 residuals tend to be consistently higher than the surges by about 1-2cm.

411 To examine the effect of non-linear interaction on the timing of the surge maximum, we also examine the total
412 water level at the time of the four largest annual maxima from the ζ_R and ζ_M . In order to do so we add the
413 predicted tide height to the surge and residuals at the times that the respective peaks occurred and again
414 ranked the two groups and plot their relationship (black points and bottom and left axes on Figure 6). In this
415 case near one to one relationships are now only seen for eight of the fourteen stations. Tide-surge interaction
416 is evident for Cape Ferguson, Rosslyn Bay, Broome, Darwin, Burnie and Stony Point. With the exception of
417 Broome, the interaction is such that the total sea level at the times of the maximum ζ_R is smaller than the total
418 sea level at times of maximum ζ_M . In other words when tides are included in the model simulations, the
419 interaction between tides and surges causes the maximum sea levels to occur during lower tides. The density
420 distribution of the tides at the time of the 4-largest surges and residuals (not shown) indicates that the reason
421 for the difference is that maximum residuals tend to occur on low waters for these locations. This 'phase
422 locking' phenomenon may occur because the presence of a surge increase the water depth and this changes the

Deleted: and

424 speed of the tidal wave due to the reduced bottom friction [e.g. *Arns et al.*, 2015]. As shown by *Horsburgh and*
425 *Wilson* [2008] in observations, a first order effect of this is that the peak surge occurs before the maximum
426 water level due to tides only.

427 From the above analysis we conclude (1) that tide-surge interaction does exist, particularly over the shallow
428 shelf areas in the northwest, northeast and Bass Strait where large tidal amplitudes enhance these interactions.
429 The interactions in these locations affect both the timing and height of the surge. The effect on timing is
430 particularly important for operational forecasting considerations. However, our analysis also shows (2) that
431 there is little overall difference in the magnitudes of the highest weather-driven events (i.e. ζ_R and ζ_M). This
432 suggests that for the remainder of this study in which we are dealing with future changes in weather
433 conditions and their effects on sea levels the omission of tidal forcing in the hydrodynamic simulations forced
434 by climate models is not likely to alter the overall conclusions regarding changes to extreme sea levels
435 [*Williams et al.*, 2016].

436

437 4. Climate change results

438 In this section, the primary focus is on changes in ESLs simulated by the climate change experiments listed in
439 Table 2. First, quantile-quantile plots between the current climate (1980-1999) CC simulations and the B-M
440 simulation are undertaken to examine the comparative performance of the different climate models under
441 present climate conditions. Then the differences between the present and future climate conditions are
442 examined.

443 4.1 Comparison with current climate

444 Figure 7 displays quantile-quantile sea level plots. They are used to compare the performance of the four CC
445 experiments over the current climate period with those from the baseline (B-M) simulation. The figure
446 suggests that the different climate models perform reasonably in modelled sea levels for the lower percentile
447 ranges. The sea level response across the upper percentile range from the climate models over the current
448 climate period is only on par with the baseline experiment for Spring Bay while Port Kembla, Cape Ferguson
449 and Portland. Rosslyn Bay, Milner Bay, Broome, Thevenard, Port Stanvac and Stony Point display lower sea
450 levels. For Darwin the lower percentiles are also overestimated by all models. Out of the four simulations CC-
451 I performs the worst for Broome, Milner Bay, Thevenard and Port Stanvac. CC-H performs the best for Port
452 Stanvac and Thevenard.

453 The average annual maximum sea levels from the B-M simulation are shown in Figure 8a together with values
454 from the tide gauges residuals over 1980-1999. From Portland to Broome (counter clockwise), the B-
455 M model is able to represent both magnitude and spatial variation in ESLs well. However at Hillarys on the
456 west coast and Albany on the southwest coast the model underestimates the extremes. This underestimation

Deleted:

458 may be partly due the contribution of wind-waves to ESLs (i.e. through wave setup), which is not considered
459 in this study. A second, potentially larger contributor is sea level variably associated with baroclinic forcing
460 and the Leeuwin Current [McInnes *et al.*, 2016]. ESLs were also underestimated in this same region in the
461 study of [Haigh *et al.*, 2014a], which, like this study, did not consider wave-driven or baroclinic processes
462 influencing sea level. Model values are also underestimated at Port Stanvac and this may be due to poor model
463 resolution of Gulf of St Vincent in which Port Stanvac is located.

464 Figure 8b shows the ensemble-average annual maximum sea levels of the four CC simulations. Results show
465 that the climate model forcing leads to overall lower sea level extremes around the coastline of Australia
466 compared to the baseline (B-M) simulation. This is likely to be at least partially due to the lower spatial and
467 temporal resolution in the CC forcing (Table 1) compared to B-M. However, the variation in the ESL
468 magnitude around the coastline is generally well captured with higher sea levels in the Gulf of Carpentaria and
469 the southeastern coastline and Tasmania compared to the east and west coast regions.

470 We note that the skill of eight CMIP5 models in reproducing variables of surface temperature, precipitation
471 and air pressure over continental areas by Watterson *et al.*, [2014], including the four used here, led to model
472 skill rankings which were markedly different to those determined by Hemer and Trenham [2015] in assessing
473 global wind-wave climate skill using wind forcing from the same models. This highlights the need to assess
474 the skill of the GCMs according to the task to which they are being used.

475 **4.2 Seasonal mean maximum sea level change**

476 To understand how seasonal changes in atmospheric forcing affect both the seasonal/ interannual and short-
477 term (storm surge) sea level variations, the average of the largest sea level events per season over each set of
478 20 seasons is calculated and the 1980-1999 average values are subtracted from those of the 2080-2099 (Figure
479 9) for each of the CC simulations. The largest positive anomalies of up to 0.1 m are seen in the Gulf of
480 Carpentaria in DJF in the CC-A and CC-H simulations. The positive anomalies extend to MAM in CC-A, are
481 also positive in CC-C but are negative by up to -0.1 m in CC-H. Along the southern mainland coastline, the
482 changes are generally small and mostly negative consistent with results reported in Colberg and McInnes
483 [2012]. However, positive changes are evident in CC-H in SON and CC-I in DJF and MAM over the
484 southeast of the mainland and Tasmania. On the east and west coastal regions, the changes across models are
485 typically small and within the range of ± 0.04 m.

486 To better understand the atmospheric forcing changes responsible for these changes in sea level variability
487 seen in the CC-A simulation between present and future time slices, the change in the seasonal mean and
488 standard deviation (STD) of the wind speed from the ACCESS1.0 is shown in Figure 10. Also shown on
489 Figure 10a is the zero contour line of the zonal wind speed from 1980-1999 (blue) and 2080-2099 (red). This
490 contour line identifies the delineation between the monsoon north-westerlies and tradewind easterlies over

491 northern Australia during DJF and the subtropical ridge separating trade easterlies from mid-latitude
492 westerlies over southern Australia throughout the year.

493 During DJF the eastward shift in the zero contour of the zonal wind in the 2080-2099 DJF is accompanied by
494 a general increase in wind speed across tropical Australia and wind STD within the Gulf of Carpentaria. This
495 suggests there is a greater influence of northeast monsoon winds on the Gulf of Carpentaria, which provide
496 favourable conditions for increased sea levels in the Gulf [*Oliver and Thompson, 2008*]. The CC-H
497 simulations produce a similar increase in sea levels in the Gulf during DJF, also related to northwest monsoon
498 winds penetrating further east and increased variability in this region. The reasons for the positive anomalies
499 in the ACCESS1.0 and the CC-C simulations in MAM are less clear since both simulations show a decrease in
500 mean winds and variability in the Gulf of Carpentaria (not shown).

501 Along the southern coastline of the continent and Tasmania there is a tendency for a decrease in ESLs in most
502 seasons of the models. As illustrated in figure 10 for CC-A, this is related to the southward movement of the
503 subtropical ridge, reduced wind variability and the greater frequency of non-storm surge producing easterly
504 winds. In CC-H in SON, positive anomalies in sea level are seen and this is related to both an increase in
505 westerlies over Tasmania and a strong increase in STD (not shown). The weak increase in CC-I in DJF is
506 related to the minimal southward movement of the mid-latitude storm belt together with an increase in the
507 STD in that model.

508 The overall projected changes to maximum ESL events around Australia are summarised in Figure 11. These
509 ensemble differences are generated by finding the difference between the maximum sea level for 1990-1999
510 and 2080-2099 time periods for each of the CC ensemble members. Since each time period is 20 years, this
511 equates to the (empirical) change in 1 in 20 year average recurrence interval; the minimum, average and
512 maximum of these ensemble differences are shown in the upper, middle and lower subplot of Figure 11 and
513 give an indication of uncertainty. Additionally, the values of ESL are hatched where the model solutions differ
514 in sign indicating inter-model variability. The minimum changes are negative around the entire coastline
515 indicating an average decrease in the approximate 20-year average recurrence interval in the range of 0 to 0.2
516 m. The largest projected decreases are on the northwestern shelf, the central west and south coasts. The
517 average change across the four models is weakly negative around most of the coastline with weak positive
518 anomalies evident along parts of the north, the GoC and southern Tasmania. The ensemble maximum changes
519 show weak positive anomalies of up to 0.04 m along the southeast and east coast. The largest positive changes
520 of up to 0.15 m occur on the eastern side of the Gulf of Carpentaria, the central north coast and parts of the
521 northwest and west coast. Negative anomalies occur on the central south and southwest coasts. Overall, model
522 results are fairly robust over the southern coastline where all models suggest a decline in maximum sea levels.
523 Large areas particularly over the north exist where changes in maximum ESL could go either way depending
524 on the atmospheric model used. This may indicate possible uncertainties in parameterizing atmospheric

525 convection in climate models over the tropics, which in turn strongly influences monsoonal winds and sea
526 level setup in the Gulf of Carpentaria. It is worth noting that *Vousdoukas et al.*, [2018] project changes for the
527 Australian coastline in a 6-member ensemble containing one model in common with the present study
528 (ACCESS1.0) and find for 2100 under RCP 8.5 largely uncertain changes in the Gulf of Carpentaria, mostly
529 negative changes around the eastern, southern and western coastlines, positive changes across Tasmania and
530 southeastern Australia and uncertain changes along the southwestern mainland coastline and the Gulf of St
531 Vincent.

522 5. Summary and Concluding Discussion

533 In order to investigate characteristics of extreme sea levels (ESLs), a depth-averaged hydrodynamic model
534 covering Australia was implemented at 5 km spatial resolution and baseline simulations carried out over the
535 period 1981 to 2012 with hourly atmospheric and tidal forcing. Overall, simulations of longer-term (seasonal
536 and interannual) and short-term (weather-driven) variations in sea level compare well with those measured at
537 tide gauges, with differences largely reflecting the absence of baroclinic forcing in the model. The modelled
538 tides agree well with observations in all except the Gulf of Carpentaria where the O1 and K1 constituents
539 were underestimated by the model and the southwestern coast where the M2 and S2 constituents were
540 underestimated. The effect of tide-surge interaction on the amplitude of the meteorological component of sea
541 level extremes (e.g. storm surge) was found to be small for much of the coastline; the main effect of the
542 interaction being on the timing of the peak sea levels rather than the annual maximum surges/residuals. This
543 suggested that in climate model-forced hydrodynamic simulations that assess how atmospheric circulation
544 changes affect ESLs, tidal forcing could be neglected. This is further supported by the finding (across a large
545 number of north Atlantic tide gauges) that while tide-surge interaction may affect the timing of maximum
546 water levels, tides have no direct effect on the magnitude of storm surge [*Williams et al.*, 2016].

547
548 Hydrodynamic simulations were carried out over the periods 1980-1999 and 2080-2099 using forcing from
549 four CMIP5 climate models run with the RCP 8.5 emission scenario. Changes in ESLs were generally small
550 and mostly negative along much of the coastline. However, in some areas ESL changes were sensitive to the
551 movement of major atmospheric circulation patterns. This was because of factors such as bathymetric depths
552 and coastline orientation in relation to the weather forcing that favoured the occurrence of certain sea level
553 extremes. For example, the Gulf of Carpentaria exhibited relatively large increases in ESLs in the climate
554 models that simulated eastward movement of the northwest monsoon during the DJF season. However, since
555 only two of the four climate model simulations simulated this change in the future climate, the finding is
556 uncertain. Along the mainland south coast, there was a greater tendency for the models to indicate a reduction
557 of ESLs in the future, particularly during winter which is also consistent with the finding of *Colberg and*
558 *McInnes* [2012] using CMIP3 and regional climate models for the atmospheric forcing and somewhat similar
559 to the study of *Vousdoukas et al.*, [2018] regional climate models for the atmospheric forcing.

Deleted: .

561

562 ~~This being the first study to examine~~ projected ESL changes ~~over the entire Australian coastline~~, we note
563 several ~~important~~ caveats. First, the changes are subject to large uncertainty due to the small number of
564 CMIP5 models used to force the hydrodynamic model. Furthermore, certain important drivers of ESLs ~~may be~~
565 poorly represented in climate models in general, e.g. tropical cyclones (TCs). ~~Previous studies [e.g. Haigh et~~
566 ~~al., 2014b] have demonstrated that numerical hindcasts (or projections) of several decades (such as the 20-~~
567 ~~year time slices used here) typically provide poor estimations of non-tidal ESL's over tropical Australia. This~~
568 ~~is due both to a lack of sufficient resolution in most available atmospheric models and the low frequency,~~
569 ~~high-impact nature of locally landfalling TCs, which generally provides low statistical confidence in related~~
570 ~~ESLs at any given location. Modelling a large numbers of synthetic cyclones [e.g. Haigh et al., 2014b,~~
571 ~~McInnes, et al., 2014] can address this shortcoming to some extent although a question in terms of statistical~~
572 ~~robustness may remain.~~ Furthermore, areas which experience high interannual and decadal sea level
573 variability may also require specialised statistical treatment and or very long model runs (i.e. greater than
574 several decades) to accurately characterise non-tidal ESLs. This is illustrated in the results presented here:
575 many areas shown to have a high dependence on ENSO variability (e.g. Figure 4 in *McInnes et al.*, [2016])
576 coincide with areas where the projected ESL changes disagree in sign in this study (Figure 11). Thus, ~~results~~
577 ~~presented here should be seen in the context of the limitations of the available data and/or downscaling~~
578 ~~techniques used. We demonstrate a robust change in ESLs over southern Australia, while future changes over~~
579 ~~tropical Australia remain largely uncertain due to the spatial resolution of CMIP5 climate models and the use~~
580 ~~of computationally tractable time slices (here 20 years).~~ Future studies may address these uncertainties by
581 better exploring the uncertainty space, e.g. by considering a larger ensemble of hydrodynamic simulations
582 forced with higher resolution climate models that better capture important small-scale meteorological features,
583 or by perturbing characteristics of historical storms to produce plausible future synthetic storm libraries
584 [*McInnes et al.*, 2014]. We also note that wind-waves contribute to sea level extremes and these effects and
585 their potential changes need to be assessed for a more complete understanding of the changes to sea level
586 extremes [e.g. *Hoeke et al.*, 2015]. The increasing availability of wave climate change assessments [e.g.
587 *Hemer et al.*, 2013; *Hemer and Trenham*, 2015] will facilitate future efforts in this regard. Also, while
588 previous studies similar to this one have focused on changes to ESLs and coastal inundation [e.g. *Colberg and*
589 *McInnes*, 2012; *McInnes et al.*, 2013], consideration of changes to other variables, including currents is
590 emerging [e.g. *Lowe et al.*, 2009]. Changes to wind-driven coastal currents, which could be considered using
591 the modelling framework presented in this study (but is beyond the scope of this paper), is also potentially
592 important in the context of coastal erosion and shoreline change [*Gornitz*, 1991; *O'Grady et al.*, 2015].

593

594

595 Acknowledgements

596

Deleted: With regards to the

Deleted: are

Deleted: (

Deleted: historical hindcast

Deleted: by

Deleted: modelled ESL's over tropical Australia are not able to represent observed ESL's very

Commented [RKH]: And due to the low frequency, high-impact nature of locally landfalling TCs....

Deleted: well due to the

Deleted: lack of resolution in the atmospheric models.

Deleted: still

Deleted: s

Deleted: R

Deleted: ed resources in terms of geophysical data for both spatial resolution and temporal scales

Deleted: particulars

Deleted: atmospheric

Deleted: forcing

Deleted: how they are presented in coarse resolution climate models

Deleted: .

617 The Australian Climate Change Science Program and the Earth System and Climate Change Hub of
618 Australian Government's National Environmental Science Program, is acknowledged for funding this
619 research. We also acknowledge the CSIRO High Performance Computing facility which provided
620 computational support for the work described in this study.
621
622

Deleted: me

624 **References**

- 625
- 626 Antony, C., and A. Unnikrishnan (2013), Observed characteristics of tide-surge interaction along the east coast of India
627 and the head of Bay of Bengal, *Estuarine, Coastal and Shelf Science*, 131, 6-11.
- 628 Arns, A., Wahl, T., Dangendorf, S., & Jensen, J. (2015), The impact of sea level rise on storm surge water levels in the
629 northern part of the German Bight. *Coastal Engineering*, 96, 118–131.
- 630 Chapman, D. C. (1985), Numerical Treatment of Cross-Shelf Open Boundaries in a Barotropic Coastal Ocean Model,
631 *Journal of physical oceanography*, 15(8), 1060-1075.
- 632 Colberg, F., and K. L. McInnes (2012), The impact of future changes in weather patterns on extreme sea levels over
633 southern Australia, *Journal of Geophysical Research: Oceans*, 117(C8), C08001.
- 634 Flather, R. A. (1976), A tidal model of the north-west European continental shelf., *Memoires de la societe Royale des*
635 *Sciences de Liege*, 10, 141-164.
- 636 Forbes, A., and J. Church (1983), Circulation in the Gulf of Carpentaria. II. Residual currents and mean sea level, *Marine*
637 *and Freshwater Research*, 34(1), 11-22.
- 638 Godfrey, J., and K. Ridgway (1985), The large-scale environment of the poleward-flowing Leeuwin Current, Western
639 Australia: longshore steric height gradients, wind stresses and geostrophic flow, *Journal of physical oceanography*,
640 15(5), 481-495.
- 641 Gordon, H., S. O'Farrell, M. Collier, M. Dix, L. Rotstayn, E. Kowalczyk, T. Hirst, and I. Watterson (2010), *The CSIRO*
642 *Mk3. 5 climate model*, CAWCR.
- 643 Gornitz, V. (1991), Global coastal hazards from future sea level rise, *Palaeogeography, Palaeoclimatology,*
644 *Palaeoecology*, 89(4), 379-398.
- 645 Green, D., L. Alexander, K. L. McInnes, J. Church, N. Nicholls, and N. White (2010), An assessment of climate change
646 impacts and adaptation for the Torres Strait Islands, *Climatic Change*, 102, 405–433.
- 647 Egbert, G. D., A. F. Bennett, and M. G. Foreman (1994), TOPEX/POSEIDON tides estimated using a global inverse
648 model, *Journal of Geophysical Research: Oceans (1978–2012)*, 99(C12), 24821-24852.
- 649 Egbert, G. D., and S. Y. Erofeeva (2002), Efficient inverse modeling of barotropic ocean tides, *Journal of Atmospheric &*
650 *Oceanic Technology*, 19(2).
- 651 Haigh, I., E. M. S. Wijeratne, L. MacPherson, C. Pattiaratchi, M. Mason, R. Crompton, and S. George (2014a),
652 Estimating present day extreme water level exceedance probabilities around the coastline of Australia: tides, extra-
653 tropical storm surges and mean sea level, *Clim Dyn*, 42, 121-138.
- 654 Haigh, I., L. MacPherson, M. Mason, E. M. S. Wijeratne, C. Pattiaratchi, R. Crompton, and S. George (2014b),
655 Estimating present day extreme water level exceedance probabilities around the coastline of Australia: tropical
656 cyclone-induced storm surges, *Clim Dyn*, 42, 139-147.
- 657 Hanson, S., R. Nicholls, N. Ranger, S. Hallegatte, J. Corfee-Morlot, C. Herweijer, and J. Chateau (2011), A global
658 ranking of port cities with high exposure to climate extremes, *Climatic Change*, 104(1), 89-111.
- 659 Hunter, J. R., Church, J. A., White, N. J., & Zhang, X. (2013), Towards a global regionally varying allowance for sea-
660 level rise. *Ocean Engineering*, 71, 17–27. <https://doi.org/10.1016/j.oceaneng.2012.12.041>
- 661 Hemer, M. A., Y. Fan, N. Mori, A. Semedo, and X. L. Wang (2013), Projected changes in wave climate from a multi-
662 model ensemble, *Nature Clim. Change*, advance online publication.

Deleted: W.

664 Hemer, M. A., & Trenham, C. E. (2016), Evaluation of a CMIP5 derived dynamical global wind wave climate model
665 ensemble. *Ocean Modelling*, 103, 190–203. <https://doi.org/10.1016/J.OCEMOD.2015.10.009>

666 Hoeke, R., McInnes, K., & O’Grady, J. (2015), Wind and Wave Setup Contributions to Extreme Sea Levels at a Tropical
667 High Island: A Stochastic Cyclone Simulation Study for Apia, Samoa. *Journal of Marine Science and Engineering*,
668 3(3), 1117–1135. <https://doi.org/10.3390/jmse3031117>

669 Horsburgh, K., and C. Wilson (2007), Tide-surge interaction and its role in the distribution of surge residuals in the North
670 Sea, *Journal of Geophysical Research: Oceans (1978–2012)*, 112(C8).

671 Jordà, G., D. Gomis, E. Álvarez-Fanjul, and S. Somot (2012), Atmospheric contribution to Mediterranean and nearby
672 Atlantic sea level variability under different climate change scenarios, *Global and Planetary Change*, 80–81(0),
673 198-214.

674 Jakobsson, M., R. MacNab, M. Mayer, R. Anderson, M. Edwards, J. Hatzky, H-W. Schenke, and P. Johnson (2008), An
675 improved bathymetric portrayal of the Arctic Ocean: Implications for ocean modeling and geological, geophysical
676 and oceanographic analyses, v. 35, L07602, *Geophysical Research Letters*, [doi:10.1029/2008GL033520](https://doi.org/10.1029/2008GL033520)

677 Jungclaus, J. H., N. Keenlyside, M. Botzet, H. Haak, J. J. Luo, M. Latif, J. Marotzke, U. Mikolajewicz, and E. Roeckner
678 (2006), Ocean Circulation and Tropical Variability in the Coupled Model ECHAM5/MPI-OM, *Journal of Climate*,
679 19(16), 3952-3972.

680 Kistler, R., et al. (2001), The NCEP–NCAR 50–Year Reanalysis: Monthly Means CD–ROM and Documentation,
681 *Bulletin of the American Meteorological Society*, 82(2), 247-267.

682 Kumar, R. K., A. K. Sahai, K. K. Kumar, S. K. Patwardhan, P. K. Mishra, J. V. Revadekar, K. Kamala, and G. B. Pant
683 (2006), High-resolution climate change scenarios for India for the 21st century, *Current Science*, 90 (3), 334-345.

684 Lin, N., K. Emanuel, M. Oppenheimer, and E. Vanmarcke (2012), Physically based assessment of hurricane surge threat
685 under climate change, *Nature Clim. Change*, 2(6), 462-467.

686 Lionello, P., D. Conte, L. Marzo, and L. Scarascia, (2017), The contrasting effect of increasing mean sea level and
687 decreasing storminess on the maximum water level during storms along the coast of the Mediterranean Sea in the
688 mid 21st century. *Global and Planetary Change*, 151, 80-91.

689 Lowe, J. A., et al. (2009), UK Climate Projections science report: Marine and coastal projections., edited, p. 96 pp, Met
690 Office Hadley Centre, Exeter, UK.

691 Marcos, M., G. Jordà, D. Gomis, and B. Pérez (2011), Changes in storm surges in southern Europe from a regional
692 model under climate change scenarios, *Global and Planetary Change*, 77(3–4), 116-128.

693 McGregor, J. L., and M. R. Dix (2008), An updated description of the conformal-cubic atmospheric model, in *High*
694 *resolution numerical modelling of the atmosphere and ocean*, edited, pp. 51-75, Springer.

695 McInnes, K. L., and G. D. Hubbert (2001), The impact of eastern Australian cut-off lows on coastal sea levels,
696 *Meteorological Applications*, 8(2), 229-243.

697 McInnes, K. L., and G. D. Hubbert (2003), A numerical modelling study of storm surges in Bass Strait, *Australian*
698 *meteorological magazine* 52 143-156

699 McInnes, K. L., Macadam, I., Hubbert, G.D. and O’Grady, J.G. (2009), A Modelling Approach for Estimating the
700 Frequency of Sea Level Extremes and the Impact of Climate Change in Southeast Australia. , *Natural Hazards* 51,
701 115–137.

702 McInnes, K. L., et al. (2012), Climate Futures for Tasmania: Extreme tide and sea-level events *Rep.*, 40 pp pp, Antarctic
703 Climate and Ecosystems CRC.

704 McInnes, K. L., I. Macadam, G. Hubbert, and J. O'Grady (2013), An assessment of current and future vulnerability to
705 coastal inundation due to sea-level extremes in Victoria, southeast Australia, *International Journal of Climatology*,
706 33(1), 33-47.

707 McInnes, K. L., K. J. E. Walsh, R. K. Hoeke, J. G. O'Grady, F. Colberg, and G. D. Hubbert (2014), Quantifying storm
708 tide risk in Fiji due to climate variability and change, *Global and Planetary Change*, 116, 115–129.

709 McInnes, K.L., Hoeke, R.K., Walsh, K.J.E., O'Grady, J.G. and Hubbert, G.D. (2016a), Tropical Cyclone Storm Tide
710 Assessment for Samoa. *Natural Hazards*. 80: 425–444. DOI 10.1007/s11069-015-1975-4

711 McInnes, K.L., White, C.J., Haigh, I.D., Hemer, M.A., Hoeke, R.K., Holbrook, N.J., Kiem, A.S., Oliver, E.C.J.,
712 Ranasinghe, R., Walsh, K.J.E., Westra, S. and Cox, R. (2016b), Natural hazards in Australia: sea level and coastal
713 extremes. *Climatic Change*. DOI: 10.1007/s10584-016-1647-8

714 Menéndez, M., and P. L. Woodworth (2010), Changes in extreme high water levels based on a quasi-global tide-gauge
715 data set, *Journal of Geophysical Research: Oceans*, 115(C10), C10011.

716 Murphy, J. M., B. B. Booth, M. Collins, G. R. Harris, D. M. H. Sexton, and M. J. Webb (2007), A methodology for
717 probabilistic predictions of regional climate change from perturbed physics ensembles, *Philosophical Transactions
718 of the Royal Society A: Mathematical, Physical and Engineering Sciences*, 365(1857), 1993-2028.

719 Nakićenović, N., and R. Swart (2000), Emission scenarios *Rep.*, 20 pp pp, Intergovernmental Panel for Climate Change

720 Nicholls, R. J., N. Marinova, J. A. Lowe, S. Brown, P. Vellinga, D. De Gusmao, J. Hinkel, and R. S. Tol (2011), Sea-
721 level rise and its possible impacts given a 'beyond 4 C world' in the twenty-first century, *Philosophical
722 Transactions of the Royal Society A: Mathematical, Physical and Engineering Sciences*, 369(1934), 161-181.

723 O'Grady, J. G., K. L. McInnes, F. Colberg, M. A. Hemer, and A. V. Babanin (2015), Longshore wind, waves and
724 currents: climate and climate projections at Ninety Mile Beach, southeastern Australia, *International Journal of
725 Climatology*, 35: 4079-4093.

726 Olbert, A., S. Nash, C. Cunnane, and M. Hartnett (2013), Tide–surge interactions and their effects on total sea levels in
727 Irish coastal waters, *Ocean Dynamics*, 63(6), 599-614.

728 Oliver, E. C. J., and K. R. Thompson (2011), Sea level and circulation variability of the Gulf of Carpentaria: Influence of
729 the Madden-Julian Oscillation and the adjacent deep ocean, *Journal of Geophysical Research: Oceans*, 116(C2),
730 C02019.

731 Pattiaratchi, C. B., and M. Eliot (2008), Sea level variability in southwest Australia: from hours to decades., in
732 *Proceedings of the 31st ASCE international conference on coastal engineering*, edited, Hamburg.

733 Pawlowicz, R., B. Beardsley, and S. Lentz (2002), Classical tidal harmonic analysis including error estimates in
734 MATLAB using T_TIDE, *Computers & Geosciences*, 28(8), 929-937.

735 Pickering, M. D., K. J. Horsburgh, J. R. Blundell, J. J. M. Hirschi, R. J. Nicholls, M. Verlaan, and N. C. Wells, 2017: The
736 impact of future sea-level rise on the global tides. *Continental Shelf Research*, 142, 50-68

737 Rossiter, J. R. (1961), Interaction Between Tide and Surge in the Thames, *Geophys J Int*, 6(1), 29-53.

738 Saha, S., et al. (2010), The NCEP Climate Forecast System Reanalysis, *Bulletin of the American Meteorological Society*,
739 91(8), 1015-1057.

740 Shchepetkin, A. F., and J. C. McWilliams (2005), The regional oceanic modeling system (ROMS): a split-explicit, free-
741 surface, topography-following-coordinate oceanic model, *Ocean Modelling*, 9(4), 347-404.

742 Sterl, A., H. van den Brink, H. de Vries, R. Haarsma, and E. van Meijgaard (2009), An ensemble study of extreme storm
743 surge related water levels in the North Sea in a changing climate, *Ocean Science*, 5(3), 369-378.

744 Taylor, K. E., R. J. Stouffer, and G. A. Meehl (2012), An Overview of CMIP5 and the Experiment Design, *Bulletin of the*
745 *American Meteorological Society*, 93(4), 485-498.

746 Tregoning, P., K. Lambeck, and G. Ramillien (2008), GRACE estimates of sea surface height anomalies in the Gulf of
747 Carpentaria, Australia, *Earth and Planetary Science Letters*, 271(1), 241-244.

748 Trenham, C. E., M. A. Hemer, T. H. Durrant, and D. J. M. Greenslade (2013), PACCSAP Wind-wave Climate: High
749 resolution windwave climate and projections of change in the Pacific region for coastal hazard assessments *Rep.*, 44
750 pp.

751 Unnikrishnan, A., M. RameshKumar, and B. Sindhu (2011), Tropical cyclones in the Bay of Bengal and extreme sea-
752 level projections along the east coast of India in a future climate scenario, *Current Science*, 101(3), 327-331.

753 Vousdoukas, M. I., E. Voukouvalas, A. Annunziato, A. Giardino, and L. Feyen, (2016), Projections of extreme storm
754 surge levels along Europe. *Climate Dynamics*, 47, 3171-3190.

755 Vousdoukas, M. I., L. Mentaschi, E. Voukouvalas, M. Verlaan, and L. Feyen, (2017), Extreme sea levels on the rise
756 along Europe's coasts. *Earth's Future*, 5, 304-323.

757 Vousdoukas, M. I., Mentaschi, L., Voukouvalas, E., Verlaan, M., Jevrejeva, S., Jackson, L. P., & Feyen, L. (2018).
758 Global probabilistic projections of extreme sea levels show intensification of coastal flood hazard. *Nature*
759 *communications*, 9(1), 2360.

760 Wahl, T., Haigh, I. D., Nicholls, R. J., Arns, A., Dangendorf, S., Hinkel, J., & Slangen, A. B. A. (2017), Understanding
761 extreme sea levels for broad-scale coastal impact and adaptation analysis. *Nature Communications*, 8, 16075.
762 <https://doi.org/10.1038/ncomms16075>

763 Williams, J., Horsburgh, K. J., Williams, J. A., and Proctor, R. N. F. (2016), Tide and skew surge independence: New
764 insights for flood risk. *Geophysical Research Letters*, 43(12), 6410–6417. <https://doi.org/10.1002/2016GL069522>

765 Wijeratne, E. M. S., C. B. Pattiaratchi, M. Eliot, and I. D. Haigh (2012), Tidal characteristics in Bass Strait, south-east
766 Australia, *Estuarine, Coastal and Shelf Science*, 114(0), 156-165.

767 Woodham, R., G.B. Brassington, R. Robertson and O. Alves (2013), Propagation characteristics of coastally trapped
768 waves on the Australian Continental Shelf: Propagation of Australian CTWS. *Journal of Geophysical Research:*
769 *Oceans*, 118(0), 4461-4473.

770 Yasuda, T., S. Nakajo, S. Kim, H. Mase, N. Mori, and K. Horsburgh (2014), Evaluation of future storm surge risk in East
771 Asia based on state-of-the-art climate change projection, *Coastal Engineering*, 83(0), 65-71.

772